Hepatic bipolar radiofrequency ablation creates coagulation zones close to blood vessels: a finite element study

D. Haemmerich[1,2] A. W. Wright[1] D. M. Mahvi[1] F. T. Lee Jr[3] J. G. Webster[2]

[1]Department of Surgery, University of Wisconsin, Madison, USA
[2]Department of Biomedical Engineering, University of Wisconsin, Madison, USA
[3]Department of Radiology, University of Wisconsin, Madison, USA

Abstract—*Radiofrequency (RF) ablation has become an important means of treatment of non-resectable primary and metastatic liver tumours. Recurrence of treated tumours is associated with cancer cell survival next to blood vessels. The paper examines the performance of classical monopolar, and two configurations of bipolar, RF ablation using a LeVeen ten-prong catheter. Finite element method models of monopolar and bipolar configurations were created at 5 mm distance from a vessel of the size of a typical portal vein (10 mm diameter). In one bipolar configuration, the probes were oriented in the same axial direction (asymmetric configuration); in the second bipolar configuration, the two probes were facing each other (symmetric configuration). The distribution of temperature and current density was analysed for three different flow conditions: normal flow, reduced flow due to portal hypertension and high flow. For normal flow, the distance between the formed coagulation zone and the blood vessel was 1.8 mm for monopolar, 1 mm for asymmetric bipolar, and 0.2 mm for symmetric bipolar, configurations. Symmetric bipolar RF ablation creates coagulation zones significantly closer to blood vessels compared with monopolar RF ablation. This may reduce tumour cell survival next to blood vessels and reduce recurrence rates.*

Keywords—*Tumour, Ablation, Radiofrequency, Finite element method*

Med. Biol. Eng. Comput., May 2003, **41**, 317–323

1 Introduction

RADIOFREQUENCY (RF) ablation has become of considerable interest as a minimally invasive treatment for primary and metastatic liver tumours (GAZELLE *et al.*, 2000). Primary *hepatocellular carcinoma* is one of the most common malignancies worldwide with, annually, around 500 000 new cases worldwide (KEW, 1985). Surgical resection offers the best chance of long-term survival, but is rarely possible. In many patients with cirrhosis or with multiple tumours, hepatic reserve is inadequate to tolerate resection, and alternative means of treatment are necessary (CURLEY*et al.*, 1997). In RF ablation, RF current is delivered to the tissue through electrodes inserted percutaneously or during surgery. Different modes of controlling the electric power delivered to tissue are utilised. Power-controlled mode ($P =$ constant), temperature-controlled mode ($T =$ constant) and impedance-controlled mode (power is applied as long as $Z <$ constant) are commonly used. The electric power is converted to heat by resistive frictional forces among ions. Tissue damage can occur at temperatures above 43 °C with long heating times of several hours; around 3 min of heating time are required at 50 °C (SAPARETO and DEWEY, 1984).

The liver is a highly perfused organ, with a dual blood supply from the hepatic artery and the portal vein. Large portal and hepatic veins are found throughout the liver parenchyma. These vessels are responsible for perfusion-mediated tissue cooling and can limit the size of the zone of necrosis caused by RF ablation (LU *et al.*, 2002; PATTERSON *et al.*, 1998). As a result, tumour cells in perivascular locations can often escape the high heat of RF ablation, and this area is responsible for a disproportionately large number of local recurrences. Despite adequate temperatures within RF lesions, local recurrence at the ablation site occurs in as many as 40% of treated tumours (ROSSI *et al.*, 1996; JIAO *et al.*, 1999; SOLBIATI *et al.*, 1997; CURLEY *et al.*, 1999).

The high recurrence rates stem partially from tumour cell survival next to large vessels and limitations in generator technology to overcome vessel-mediated cooling. In a report of recurrences after RF ablation, the majority were noted as being next to large blood vessels (GILLAMS and LEES, 1999). The lowest rate of local recurrence reported to date (less than 5%) was noted in a series of patients treated with RF ablation during a Pringle manoeuver (occlusion of vascular flow to the liver) (CURLEY *et al.*, 1999). The cooling effects of large blood vessels and vascular perfusion thus were minimised by

Correspondence should be addressed to Professor J G Webster; email: webster@engr.wisc.edu

Paper received 9 July 2002 and in final form 20 January 2003
MBEC online number: 20033775

this manoeuver. However, the Pringle manoeuver requires a major surgical procedure, which negates one of the major advantages of RF ablation, its use in a minimally invasive fashion (percutaneous or laparoscopic) (DELVA *et al.*, 1989). Vaso-active pharmacological agents have also been used to reduce blood flow to the liver (GOLDBERG *et al.*, 1998*a*) to reduce the blood cooling effect.

It has been previously shown that bipolar RF ablation between separated electrodes can create larger RF lesions using needle electrodes (CURLEY *et al.*, 1997; BURDIO *et al.*, 1999; MCGAHAN *et al.*, 1996). We showed previously, with four-prong electrodes*, that multi-prong probes can create larger RF lesions in bipolar mode. From our previous studies, it became evident that more than four prongs are desirable for bipolar application, so that current is more effectively concentrated in the region between the probes to heat this region preferentially (HAEMMERICH *et al.*, 2001; 2002). Therefore we used a different, commercially available probe with ten prongs† for this study.

We created finite element method (FEM) models of monopolar and bipolar RF ablation, with the ten-prong electrodes next to a blood vessel the size of a typical human portal vein. We compared current density, temperature distribution and distance between RF lesion and vessel wall for monopolar and two bipolar configurations to determine if a bipolar configuration had the potential to decrease the high tumour recurrence rate adjacent to hepatic blood vessels. We further investigated the effect of different flow conditions in the vessel on RF lesion formation for normal flow, reduced flow due to portal hypertension (which occurs in patients with cirrhosis) and high flow.

2 Materials and methods

2.1 *Bioheat equation*

Joule heating arises when an electric current passes through a conductor. Electric power is converted into heat. The heating of tissue during RF ablation is governed by the bioheat equation introduced by PENNES (1948)

$$\rho c \frac{\partial T}{\partial t} = \nabla \cdot k \nabla T + \boldsymbol{J} \cdot \boldsymbol{E} - h_{bl}(T - T_{bl}) - Q_m$$

$$h_{bl} = \rho_{bl} c_{bl} w_{bl}$$

where ρ is the density ($\mathrm{kg\,m^{-3}}$), c is the specific heat ($\mathrm{J\,(kg \cdot K)^{-1}}$), and k is the thermal conductivity ($\mathrm{W\,(m \cdot K)^{-1}}$). J is the current density ($\mathrm{A\,m^2}$), and E is the electric field intensity ($\mathrm{V\,m^{-1}}$). T_{bl} is the temperature of blood, ρ_{bl} is the blood density ($\mathrm{kg\,m^{-3}}$), c_{bl} is the specific heat of the blood ($\mathrm{J\,(kg \cdot K)^{-1}}$), and w_{bl} is the blood perfusion ($\mathrm{s^{-1}}$). h_{bl} is the convective heat transfer coefficient accounting for the blood perfusion. Q_m ($\mathrm{W\,m^{-3}}$) is the energy generated by metabolic processes and was neglected as it is small compared with the other terms.

In the Pennes model described in the bioheat equation, the energy exchange between blood and tissue is modelled as a non-directional heat source. One major assumption was that the heat transfer related to perfusion between tissue and blood occurs in the capillary bed, which turned out not to be fully correct. The main thermal equilibrium process takes place in the pre- or post-capillary vessels. Nevertheless, the Pennes model describes blood perfusion with acceptable accuracy, if no large vessels are nearby (ARKIN *et al.*, 1994). The blood perfusion in hepatic tissue used in the FEM model was $w_{bl} = 6.4 \times 10^{-3}\ \mathrm{s^{-1}}$ (EBBINI *et al.*, 1988).

*RITA Medical Systems, Mountain View, CA, USA

†Distributed by RadioTherapeutics, Sunnyvale, CA, USA

2.2 *Blood vessel heat transfer*

In our model, we included a vessel with 10 mm diameter, which is the typical size of the portal vein (GRAY, 1990). We set the temperature of the blood vessel to 37 °C as an additional boundary condition in our initial models. This can be considered the worst case (i.e. very high heat transfer coefficient between vessel and tissue). Later, we considered different flow velocities in the vessel. We assumed thermally and hydrodynamically fully developed flow in the vessel, which resulted in a constant heat transfer coefficient between vessel and tissue. The normal flow velocity in the portal vein is $22.9\ \mathrm{cm\,s^{-1}}$ (CIONI *et al.*, 1992). *Hepatocellular carcionoma* often appear in patients with liver cirrhosis. In these cases, portal venous blood velocity can be reduced significantly owing to portal hypertension, with an average flow velocity of $16.9\ \mathrm{cm\,s^{-1}}$ (CIONI *et al.*, 1992). Below, we estimate the heat transfer coefficient for normal and reduced portal venous blood velocity.

SHAH *et al.* (1976) determined the heat transfer coefficient for constant vessel wall temperature. Their results for the local Nusselt number can be approximated, within 3.5%, by (CHATO, 1980)

$$\mathrm{Nu}_D = 4 + 0.48624 \ln^2 [\mathrm{Re} \times \mathrm{Pr} \times D/(18 \times L)]$$

$$\mathrm{Re} = \rho_b V_b D/\mu$$

where Re is the Reynolds number, Pr is the Prandtl number (Pr = 25 for blood), D is the vessel diameter, L is the vessel length, ρ_b is the mass density of blood, μ is the viscosity of blood, V_b is the average blood velocity, and k_b is the thermal conductivity of blood. With the typical length of the portal vein of 70 mm (GRAY, 1990), we can calculate the Nusselt number for normal flow ($\mathrm{Nu}_D = 16.2$) and for portal hypertension due to cirrhosis ($\mathrm{Nu}_D = 12.8$). We can now calculate the heat transfer coefficients for the two cases with

$$h = \mathrm{Nu}_D k_b / D$$

The heat transfer coefficient is $h = 810\ \mathrm{W\,(m^2 \cdot K)^{-1}}$ for normal flow and $h = 639\ \mathrm{W\,(m^2 \cdot K)^{-1}}$ for reduced flow due to portal hypertension. We created models where we assigned these heat transfer coefficients to the vessel–tissue boundary and determined the RF lesion dimensions for these different flow conditions.

2.3 *Finite element method*

We created 3D finite element method (FEM) models for monopolar and bipolar ablation. For all FEM analyses, we used a LeVeen ten-prong probe with 3 cm diameter (when prongs are extended). The prongs are of rectangular cross-section, measuring 0.4 mm × 0.3 mm (width × height). The shaft is 2.3 mm in diameter and is insulated; only the tines conduct current. In the bipolar configuration, the two probes are

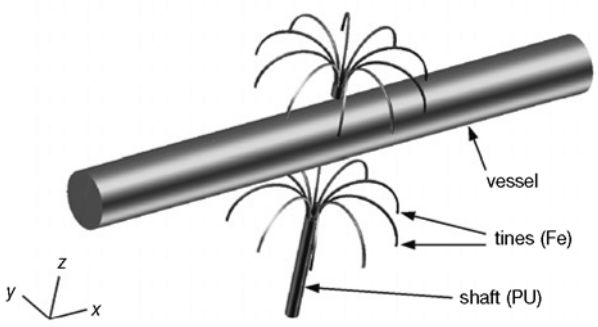

Fig. 1 *Geometry of asymmetric bipolar model*

Table 1 Material properties used in FEM

Element	Material	ρ, kg m^{-3}	c, J (kg · K)$^{-1}$	k, W (m · K)$^{-1}$	σ, S m^{-1} at 500 kHz
tines	Fe	21500	132	71	4×10^{6}
shaft	polyurethane	70	1045	0.026	10^{-5}
blood	blood	1000	4180	0.543	0.667
tissue	liver	1060	3600	0.512	0.333

placed 20 mm apart, with the vessel centred in between (i.e. the vessel is 5 mm away from the probes).

We created three different geometrical configurations: monopolar, asymmetric bipolar and symmetric bipolar. Fig. 1 shows the geometry of the probe model for the asymmetric bipolar configuration, where both probes are oriented in the same axial direction. In the bipolar configurations, current flowed between the two probes (i.e. one of the probes was assigned to ground potential). In the monopolar configuration, only the lower probe was present next to the blood vessel, and ground potential was assigned to the model boundaries. In the symmetric bipolar configuration, the upper probe was rotated by 180°, i.e. the two probes were positioned contra-axially.

We created an additional model using the symmetric bipolar configuration, where we altered the conductivity of the blood inside the vessel to be the same as tissue conductivity. In all models, probes and vessel were surrounded by a cylinder of liver tissue, 100 mm long and 100 mm in diameter. Owing to the symmetry of the arrangement, we could reduce computing time by only modelling half of the geometry shown in Fig. 1. Table 1 lists the material properties used in the model, which were taken from the literature (PANESCU *et al.*, 1995; VALVANO *et al.*, 1985). We set the initial temperature of the liver tissue and the temperature at the boundary of the model to 37 °C. Blood perfusion was modelled according to the PENNES (1948) model.

In clinical applications, the amount of power applied to the LeVeen probe is controlled by impedance control; i.e. the power is reduced once the impedance rises a certain amount above baseline impedance owing to desiccation and vaporisation (MCGAHAN and DODD, 2001). However, we were unable to simulate this process in our FEM models, owing to lack of information on the change in tissue properties above 100 °C. We used temperature control in such a way that the maximum temperature within hepatic tissue was kept at 95 °C for the duration of the treatment. We simulated ablation for 12 min; in our models, we did not observe any significant change in coagulation zone dimensions beyond that time. The maximum temperature of hepatic tissue was kept at 95 °C by varying the voltage applied to the electrodes. The RF lesion size was determined using the 50 °C margin (i.e. tissue above 50 °C is considered destroyed) at the end of the simulation.

The bipolar FEM models consisted of ~255 000 tetrahedral elements; the monopolar model consisted of ~160 000 tetrahedral elements. We used a non-uniform mesh; mesh size was 0.2 mm close to the probe, where we see large temperature and current gradients, and 5 mm at the model boundaries. We used PATRAN Version 2000‡ to generate the geometric models, assign material properties, assign boundary conditions and perform meshing. After creating the model, PATRAN generates an input file for the ABAQUS/Standard 5.8** solver. A coupled thermo-electrical analysis was performed by ABAQUS. For post-processing, we used the built-in module ABAQUS/POST to generate profiles of temperature and electric field intensity. All analysis was performed on an HP-C180 workstation equipped with 1.1 GB of RAM and 34 GB of hard disk space.

‡The MacNeal-Schwendler Co., Los Angeles, CA, USA

**Hibbitt, Karlsson & Sorensen, Inc., Pawtucket, RI, USA

3 Results

We generated FEM models of monopolar and bipolar ablation and analysed the distribution of temperature and current density distribution at the end of a 12 min ablation simulation. Temperature distributions are shown for the worst-case scenario, where blood vessel temperature is constant at 37 °C ($h \rightarrow \infty$).

Temperature and current density maps were generated for two planes. Plane 1 was oriented perpendicular to the blood vessel axis, through the catheter axis (parallel to x, z-plane in Fig. 1); plane 2 was oriented through the vessel axis (i.e. along the vessel) and through the catheter axis (parallel to y, z-plane in Fig. 1). Owing to the probe geometry, plane 1 cut through the tines, whereas plane 2 cut in between two neighbouring tines. Figs 2 and 3 show the temperature map for the monopolar configuration in plane 1 and plane 2, respectively.

Fig. 4 shows the current density map for the monopolar configuration in plane 1. Fig. 5 shows the temperature map for the asymmetric bipolar configuration in plane 1. Only the upper tine tips reach the set temperature of 95 °C, whereas the lower tine tips only reach around 70 °C. Figs 6 and 7 show the

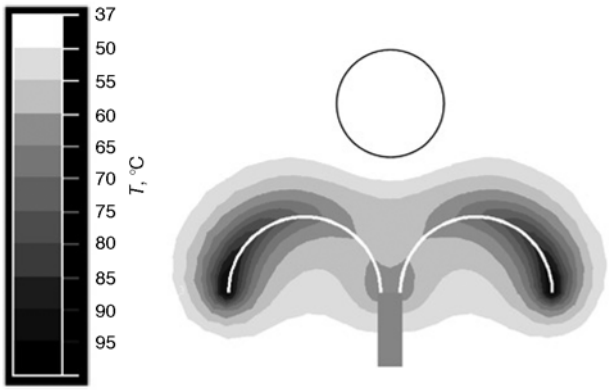

Fig. 2 *Temperature map of monopolar configuration in plane 1. Circle represents vessel wall, grey block represents shaft, and white arcs represent tines. Outermost grey border marks 50 °C margin*

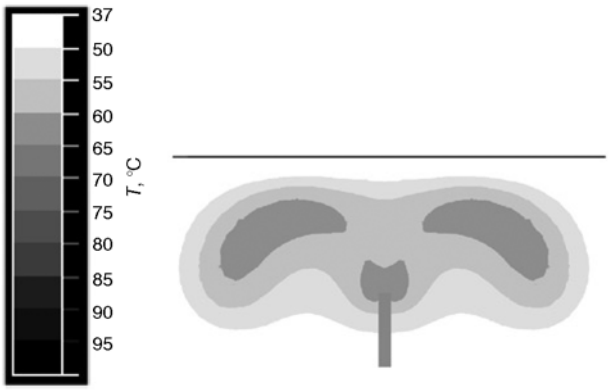

Fig. 3 *Temperature map of monopolar configuration in plane 2. Line represents vessel wall. Outermost grey border marks 50 °C margin*

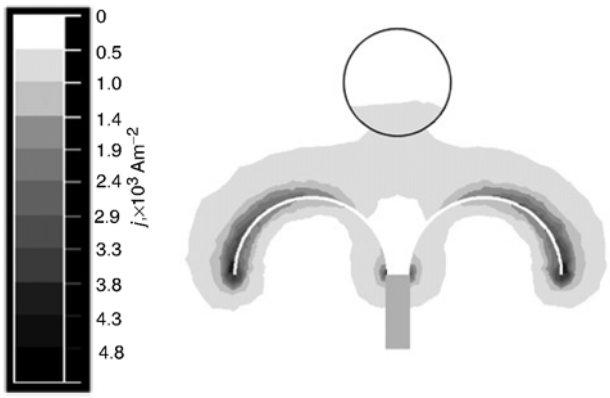

Fig. 4 *Current density map of monopolar configuration in plane 1. Circle represents vessel wall, grey block represents shaft, and white arcs represent tines*

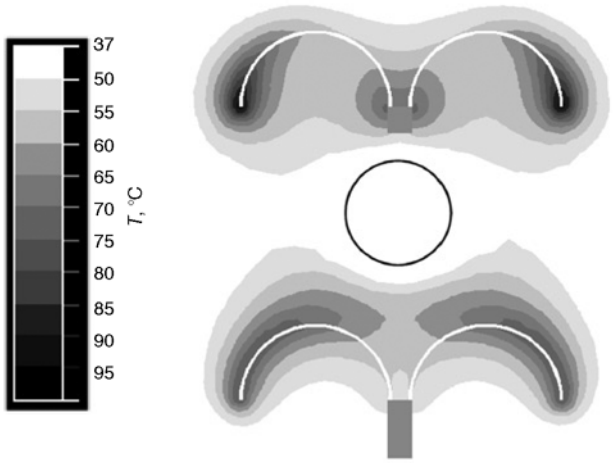

Fig. 5 *Temperature map of asymmetric bipolar configuration in plane 1. Circle represents vessel wall, grey block represents shaft, and white arcs represent tines. Outermost grey border marks 50 °C margin*

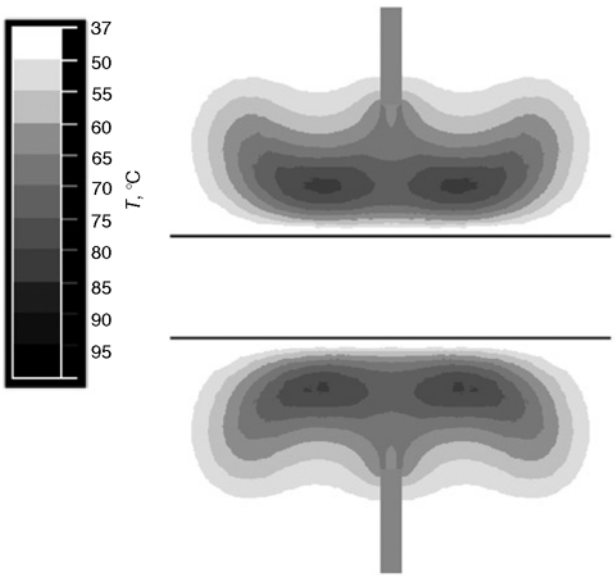

Fig. 6 *Temperature map of symmetric bipolar configuration in plane 2. Lines represent vessel wall, and grey block represents shaft. Outermost grey border marks 50 °C margin*

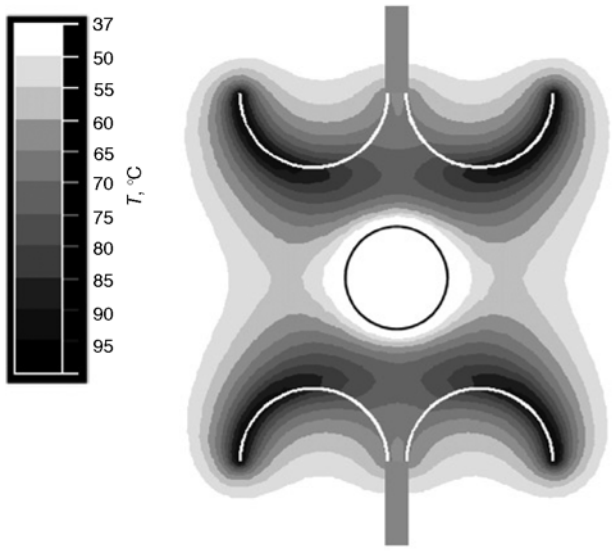

Fig. 7 *Temperature map of symmetric bipolar configuration in plane 1. Circle represents vessel wall, grey block represents shaft, and white arcs represent tines. Outermost grey border marks 50 °C margin*

temperature maps for the symmetric bipolar configuration in plane 1 and plane 2, respectively. Fig. 8 shows the temperature map in plane 1 for the symmetric bipolar configuration, where blood conductivity inside the vessel has been altered to be the same as tissue conductivity. The distance between RF lesion and vessel for the model with modified blood conductivity is 1.2 mm in the vertical direction and 1.8 mm in horizontal direction.

Fig. 9 shows the current density map for the symmetric bipolar configuration in plane 1. Fig. 10 shows the current density map for the symmetric bipolar configuration with altered blood conductivity in plane 1. For normal flow, the distance between the formed coagulation zone and the blood vessel was 1.8 mm for monopolar, 1 mm for asymmetric bipolar and 0.2 mm for symmetric bipolar configuration. Table 2 summarises the distance between RF lesion and vessel for different probe configurations and different flow conditions: normal flow ($h = 810$ W $(m^2 \cdot K)^{-1}$), reduced flow due to portal hypertension ($h = 639$ W $(m^2 \cdot K)^{-1}$) and high flow ($h \rightarrow \infty$).

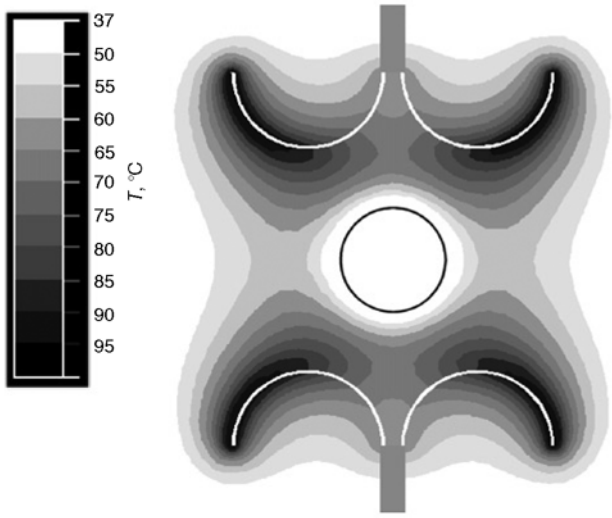

Fig. 8 *Temperature map of symmetric bipolar configuration in plane 1. Blood conductivity is altered to be same as tissue conductivity. Circle represents vessel wall, grey block represents shaft, and white arcs represent tines. Outermost grey border marks 50 °C margin*

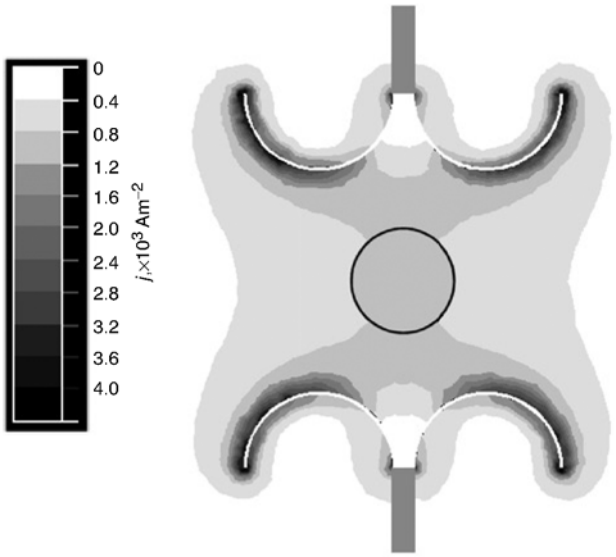

Fig. 9 *Current density map of symmetric bipolar configuration in plane 1. Circle represents vessel wall, grey block represents shaft, and white arcs represent tines.*

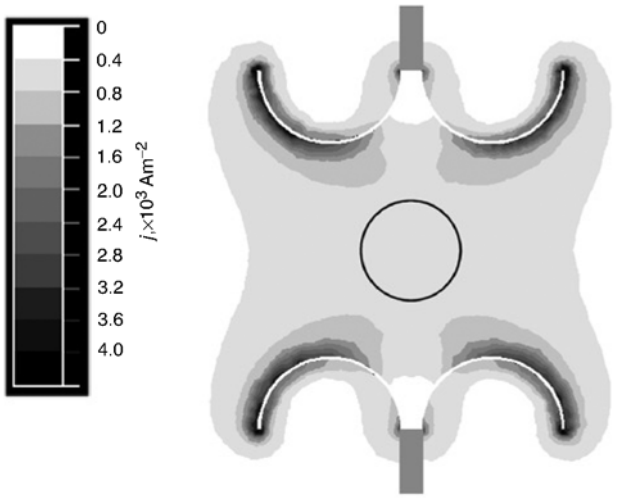

Fig. 10 *Current density map of symmetric bipolar configuration in plane 1. Blood conductivity is altered to be same as tissue conductivity. Circle represents vessel wall, grey block represents shaft, and white arcs represent tines*

4 Discussion

It is well known that cooling mediated by large blood vessels has a major impact on RF lesion formation during hepatic RF ablation (LU *et al.*, 2002; PATTERSON *et al.*, 1998; GOLDBERG *et al.*, 1998*b*). More specifically, tumour recurrence is associated with incomplete destruction of cancer cells close to blood vessels (GILLAMS and LEES, 1999). We examined the performance of bipolar RF ablation next to a large blood vessel compared with monopolar RF ablation. Figs 2 and 3 show the temperature distribution at the end of ablative treatment for the monopolar configuration, which is currently used clinically. Figs 2 and 3 show a large deflection of the RF lesion caused by the vessel. This may result in sub-optimum heating of a tumour located close to this vessel, ultimately leading to a lack of complete destruction or tumour recurrence.

We compared two methods of bipolar RF ablation using the same probe used in the monopolar configuration. First, we examined the asymmetric bipolar configuration. The RF lesion created by the lower probe showed less deflection and extended closer to the vessel compared with the monopolar configuration. Only the upper tines reached set temperature, with much lower temperature observed at the lower tine tips (see Fig. 5). This stems from the asymmetry of the configuration, where the upper probe tines point towards the lower probe and therefore create higher current density at the tine tips in contrast to the lower tine tips, which point away from the upper probe. The upper probe tines greatly limit the total amount of energy that can be dissipated by the two probes.

A large improvement over the asymmetric bipolar configuration is achieved by inverting the upper probe, which leads to a symmetric bipolar configuration (Figs 6 and 7). We now observe a confluent RF lesion surrounding the blood vessel, and the RF lesion extends much closer to the vessel compared with the asymmetric bipolar configuration. Owing to the symmetry, the tines of both probes now reach the set temperature.

The superior performance of the bipolar configuration is partially caused by the thermally synergistic effect owing to the simultaneous creation of two RF lesions close to each other. Two probes in close proximity to each other create a larger lesion than two separate lesions created by a single probe. This effect has been previously observed during microwave ablation using multiple probes (WRIGHT *et al.*, 2001). A second effect is the increased current density between the two probes. In previous experiments, where we evaluated the performance of bipolar RF ablation using four-tine multi-prong probes, we observed only a negligible increase in current density in between the probes (HAEMMERICH *et al.*, 2001). However, with the ten-tine probes used in this study, we see a substantial increase in current density between the probes compared with the monopolar configuration (see Figs 4 and 9).

Table 2 Lesion–vessel distance for different flow conditions and probe configurations. Lesion distance is given in vertical direction (along probe axis) and horizontal direction (perpendicular to probe axis)

Flow condition	Direction	Monopolar	Bipolar asymmetric	Bipolar symmetric
Portal hypertension				
$h = 639$ W $(m^2 \cdot K)^{-1}$	vertical	1.4 mm	0.5 mm	0
	horizontal	∞	∞	1.2 mm
Normal				
$h = 810$ W $(m^2 \cdot K)^{-1}$	vertical	1.8 mm	1 mm	0.2 mm
	horizontal	∞	∞	1.5 mm
Worst case				
$h \rightarrow \infty$	vertical	2.3 mm	1.8 mm	1 mm
	horizontal	∞	∞	2.3 mm

Owing to the increase in current density between the probes, the zone of active heating (i.e. not considering RF lesion formation caused by thermal conduction) extends further towards the collateral probe (i.e. towards the blood vessel). This effect may contribute substantially to the lesion extending closer to the vessel. This confirms the hypothesis of HAEMMERICH *et al.* (2001) that bipolar RF ablation using multi-prong probes is more effective, the more tines the probe has, in that it causes a more significant increase in current density between the two probes.

However, the increase in current density between the probes seen in Fig. 9 could be partially due to the blood vessel located between the probes. Blood has a much higher conductivity than liver tissue (see Table 1). Therefore current paths preferentially go through the vessel, resulting in a 'channelling' effect (see Fig. 9). This effect is smaller for smaller vessel sizes, as then the area of blood is also smaller. To examine the significance of the channelling of current caused by the vessel, we modified the symmetric bipolar model by altering the conductivity of the blood inside the vessel to be the same as the tissue conductivity (see Figs 8 and 10). We only observed a slight change in RF lesion appearance for the modified model (Fig. 8) compared with the original model (Fig. 7). The RF lesion of the modified model is slightly closer to the vessel in the horizontal direction and slightly further away from the vessel in the vertical direction. This is the result of the absence of current channelling in the modified model (Fig. 10), which was present in the original model (Fig. 9). Nevertheless, we still obtain a confluent RF lesion surrounding the vessel and conclude that the symmetric bipolar configuration creates RF lesions much closer to a blood vessel, largely independent of the vessel-mediated current channelling effect.

A disadvantage of the symmetric bipolar configuration is that the two RF probes need to be inserted from two opposing sides, which may not always be possible. A single catheter that contains two sets of tines is better from a clinical standpoint (the insertion would only require a single insertion into the liver parenchyma). Comparably, the asymmetric bipolar configuration is much simpler to implement in practice. Two catheters can be easily lined up axially and introduced together into the tissue. However, the asymmetric bipolar configuration exhibits inferior performance.

For each probe configuration, we also estimated the heat transfer between vessel and tissue for normal flow and for reduced flow due to portal hypertension. In these cases, the RF lesion extends closer to the vessel compared with the worst-case scenario (see Table 2). Flow velocity has a significant effect on RF lesion formation. For symmetric bipolar ablation in the reduced flow scenario, the RF lesion extends up to the vessel wall. In reality, both monopolar and bipolar RF ablation could create continuous RF lesions up to the vessel wall, depending on the distance between vessel and probe, vessel size and blood flow rate. Nevertheless, we showed that bipolar RF ablation is more effective in creating RF lesions next to a vessel.

5 Conclusions

We evaluated the clinically used monopolar configuration and asymmetric and symmetric bipolar configurations in close proximity to a large blood vessel. The symmetric bipolar configuration created an RF lesion fully encompassing the vessel. The RF lesion was also closest to the blood vessel, but the symmetric bipolar method may be difficult to apply in practice without substantial probe modifications. The asymmetric bipolar method performed better than the monopolar method, but only the upper probe reached a set temperature, and this therefore limited power deposition by the lower probe. No confluent RF lesion was produced. The monopolar method showed the worst performance.

We conclude that the use of bipolar RF ablation may reduce recurrence rates associated with tumour cell survival close to blood vessels by increasing current density and heat deposition in the perivascular spaces. In large vessels with high flow, even bipolar RF ablation may not create lesions up to the vessel walls and result in tumour cell survival. Therefore, although the ablation closer to blood vessels is beneficial, this may not ultimately change clinical outcome, given that, even with bipolar ablation, some residual tumour can persist. The modelling results presented will need to be verified in animal models with implantable tumours placed in close proximity to blood vessels prior to RF ablation.

Acknowledgments—This work was supported by the National Institutes of Health (NIH) under grants HL56143 and DK58839.

References

ARKIN, H., XU, L. X., and HOLMES, K. R. (1994): 'Recent developments in modeling heat transfer in blood perfused tissues', *IEEE Trans. Biomed. Eng.*, **41**, pp. 97–107

BURDIO, F., GUEMES, A., BURDIO, J. M., CASTIELLA, T., DE GREGORIO, M. A., LOZANO, R., and LIVRAGHI, T. (1999): 'Hepatic lesion ablation with bipolar saline-enhanced radiofrequency in the audible spectrum', *Acad. Radiol.*, **6**, pp. 680–686

CHATO, J. (1980): 'Heat transfer to blood vessels', *ASME Trans. Biomed. Eng.*, **102**, pp. 110–118

CIONI, G., D'ALIMONTE, P., CRISTANI, A., VENTURA, P., ABBATI, G., TINCANI, E., ROMAGNOLI, R., and VENTURA, E. (1992): 'Duplex-Doppler assessment of cirrhosis in patients with chronic compensated liver disease', *J. Gastroenterol. Hepatol.*, **7**, pp. 382–384

CURLEY, S. A., DAVIDSON, B. S., FLEMING, R. Y., IZZO, F., STEPHENS, L. C., TINKEY, P., and CROMEENS, D. (1997): 'Laparoscopically guided bipolar radiofrequency ablation of areas of porcine liver', *Surg. Endosc.*, **11**, pp. 729–733

CURLEY, S. A., IZZO, F., DELRIO, P., ELLIS, L. M., GRANCHI, J., VALLONE, P., FIORE, F., PIGNATA, S., DANIELE, B., and CREMONA, F. (1999): 'Radiofrequency ablation of unresectable primary and metastatic hepatic malignancies', *Ann. Surg.*, **230**, pp. 1–8

DELVA, E., CAMUS, Y., and NORDLINGER, B. (1989): 'Vascular occlusions for liver resections', *Ann. Surg.*, **209**, pp. 297–304

EBBINI, E. S., UMEMURA, S.-I., IBBINI, M., and CAIN, C. A. (1988): 'A cylindrical-section ultrasound phased-array applicator for hyperthermia cancer therapy', *IEEE Trans. Biomed. Eng.*, **35**, pp. 561–572

GAZELLE, G. S., GOLDBERG, S. N., SOLBIATI, L., and LIVRAGHI, T. (2000): 'Tumor ablation with radio-frequency energy', *Radiology*, **217**, pp. 633–646

GILLAMS, A. R., and LEES, W. R. (1999): 'The importance of large vessel proximity in thermal ablation of liver tumours', *RSNA 1999*, Chicago, IL, USA

GOLDBERG, S. N., HAHN, P. F., HALPERN, E. F., FOGLE, R. M., and GAZELLE, G. S. (1998*a*): 'Radio-frequency tissue ablation: effect of pharmacologic modulation of blood flow on coagulation diameter', *Radiology*, **209**, pp. 761–767

GOLDBERG, S. N., HAHN, P. F., TANABE, K. K., MUELLER, P. R., SCHIMA, W., ATHANASOULIS, C. A., COMPTON, C. C., SOLBIATI, L., and GAZELLE, G. S. (1998*b*): 'Percutaneous radiofrequency tissue ablation: does perfusion-mediated tissue cooling limit coagulation necrosis?', *J. Vasc. Interv. Radiol.*, **9**, pp. 101–111

GRAY, S. (1990): 'Gray's anatomy' (Vintage Books, New York, 1990)

HAEMMERICH, D., STAELIN, S. T., TUNGJITKUSOLMUN, S., LEE, F. T. Jr., MAHVI, D. M., and WEBSTER, J. G. (2001): 'Hepatic bipolar radiofrequency ablation between separated multiprong electrodes', *IEEE Trans. Biomed. Eng.*, **48**, pp. 1145–1152

HAEMMERICH, D., TUNGJITKUSOLMUN, S., STAELIN, S. T., LEE, F. T., Jr., MAHVI, D. M., and WEBSTER, J. G. (2002): 'Finite-element analysis of hepatic multiple probe radio-frequency ablation', *IEEE Trans. Biomed. Eng.*, **49**, pp. 836–842

JIAO, L. R., HANSEN, P. D., HAVLIK, R., MITRY, R. R., PIGNATELLI, M., and HABIB, N. (1999): 'Clinical short-term results of radiofrequency ablation in primary and secondary liver tumors', *Am. J. Surg.*, **177**, pp. 303–306

KEW, M. C. (1985): 'The development of hepatocellular carcinoma in humans', *Cancer Surv.*, **5**, pp. 719–739

LU, D. S., RAMAN, S. S., VODOPICH, D. J., WANG, M., SAYRE, J., and LASSMAN, C. (2002): LU, D. S., WANG, M. P., VODOPICH, D. J., and RAMAN, S. S. (2000): 'Effect of vessel size on creation of hepatic radiofrequency lesions in pigs: assessment of the "heat sink" effect', *Am. J. Roentgenol.*, **178**, pp. 147–156

MCGAHAN, J. P., GU, W.-Z., BROCK, J. M., TESLUK, H., and JONES, C. D. (1996): 'Hepatic ablation using bipolar radiofrequency electrocautery', *Acad. Radiol.*, **3**, pp. 418–422

MCGAHAN, J. P., and DODD, G. D., III (2001): 'Radiofrequency ablation of the liver: current status', *AJR*, **176**, pp. 3–16

PANESCU, D., WHAYNE, J. G., FLEISCHMAN, S. D., MIROTZNIK, M. S., SWANSON, D. K., and WEBSTER, J. G. (1995): 'Three-dimensional finite element analysis of current density and temperature distributions during radio-frequency ablation', *IEEE Trans. Biomed. Eng.*, **42**, pp. 879–890

PATTERSON, E. J., SCUDAMORE, C. H., OWEN, D. A., NAGY, A. G., and BUCZKOWSKI, A. K. (1998): 'Radiofrequency ablation of porcine liver *in vivo*: effects of blood flow and treatment time on lesion size', *Ann. Surg.*, **227**, pp. 559–565

PENNES, H. H. (1948): 'Analysis of tissue and arterial blood temperatures in resting forearm', *J. Appl. Phys.*, **1**, pp. 93–122

ROSSI, S., DI STASI, M., BUSCARINI, E., QUARETTI, P., GARBAGNATI, F., SQUASSANTE, L., PATIES, C. T., SILVERMAN, D. E., and BUSCARINI, L. (1996): 'Percutaneous RF interstitial thermal ablation in the treatment of hepatic cancer', *Am. J. Roentgenol.*, **167**, pp. 759–768

SAPARETO, S. A., and DEWEY, W. C. (1984): 'Thermal dose determination in cancer therapy', *Int. J. Radiat. Oncol. Biol. Phys.*, **10**, pp. 787–800

SOLBIATI, L., IERACE, T., GOLDBERG, S. N., SIRONI, S., LIVRAGHI, T., FIOCCA, R., SERVADIO, G., RIZZATTO, G., MUELLER, P. R., DEL MASCHIO, A., and GAZELLE, G. S. (1997): 'Percutaneous US-guided radiofrequency tissue ablation of liver metastases: treatment and follow-up in 16 patients', *Radiology*, **202**, pp. 195–203

VALVANO, J. W., COCHRAN, J. R., and DILLER, K. R. (1985): 'Thermal conductivity and diffusivity of biomaterials measured with self-heating thermistors', *Int. J. Thermophys.*, **6**, pp. 301–311

WRIGHT, A. W., LEE, F. T., Jr., JOHNSON, C. D., and MAHVI, D. M. (2001): 'Microwave ablation of hepatic tissue: simultaneous use of multiple probes results in large areas of tissue necrosis', *RSNA 2001*, Chicago, IL, USA

Author's biography

DIETER HAEMMERICH received the MS degree from the Department of Electrical and Computer Engineering, Technical University of Vienna, Austria in 2000, and the MS and the PhD from the Department of Biomedical Engineering, University of Wisconsin, Madison, WI in 2000 and 2001, respectively. He is currently an assistant scientist in the Department of Surgery, University of Wisconsin, Madison, WI. His research interests include finite element analysis of radio frequency ablation and tissue impedance measurement.